JPG Journal of Petroleum Geology www.jpg.co.uk

Journal of Petroleum Geology, Vol. 43(2), April 2020, pp 209-224

SEISMIC EVENTS IN THE UPPER MIOCENE – PLIOCENE SEDIMENTARY SUCCESSION IN THE GULF OF İZMİR (WESTERN ANATOLIA): IMPLICATIONS FOR HYDROCARBON PROSPECTIVITY

Z. Altan[1,*], N. Ocakoğlu[1], G. Böhm[2] and K. Tuncer Sarıkavak[3]

An analysis of multi-channel seismic reflection data integrating reflection tomography, pre-stack depth migration, AVO analysis, seismic modelling and seismic attribute analysis was used to investigate the Miocene – Quaternary stratigraphy of the Gulf of İzmir, western Anatolia. In this area, the east-west oriented Gediz graben intersects with the NE-SW oriented Bakırçay Graben. A velocity-depth model together with pre-stack depth migration allowed two seismic stratigraphic units (SSU1 and SSU2) to be distinguished. These units can be correlated with the stratigraphic succession at the offshore Foça-1 well and correspond to the Upper Miocene to Recent Bozköy, Ularca and Bayramiç Formations with a combined thickness of 1.75 km. The units rest on acoustic basement (SSU3) which has a basin-and-ridge morphology, and which corresponds to the Lower-Middle Miocene Yuntdağ Volcanics. A number of lateral velocity variations were identified. In particular, a ~90 m wide and ~500 m long lenticular-shaped low-velocity zone with an interval velocity of 1.68 km/s was identified in the Quaternary Bayramiç Formation. The structure is bounded by negative reflections whose amplitude increases with offset at the top and by strong positive reflections whose amplitude increases with offset at the base, interpreted as possible bright and flat spots respectively. These amplitude events point to the presence of gas-saturated sediments within the study area. The lenticular structure is bounded by strike-slip faults on either side, and by a Miocene – Pliocene unconformity surface below and by shales of the Bayramiç Formations above. It is therefore interpreted as a possible structural – stratigraphic trap. The strike-slip faults may allow the migration of hydrocarbons from source rocks located at greater depths. The presence of a low-velocity zone above the lenticular structure reaching up to seafloor may indicate the upward leakage of hydrocarbons from the trap. These observations will contribute to future hydrocarbon exploration activities in the study area.

[1] Istanbul Technical University (ITU), Faculty of Mines, Department of Geophysical Engineering, Turkey.
[2] Istituto Nazionale di Oceanografia e Geofisica Sperimentale (OGS), Italy.
[3] Mineral Research and Exploration General Directorate (MTA), Turkey.

* corresponding author: zaltan@itu.edu.tr

Key words: Direct hydrocarbon indicator, low velocity zone, reflection tomography, pre-stack depth migration, AVO analysis, Gulf of Izmir, Western Anatolia, Turkey.

INTRODUCTION

Western Turkey and the adjacent Aegean Sea have undergone north-south extension since the Neogene resulting in crustal thinning and an elevated heat flow regime. The horst-graben architecture of the region is one of the most common tectonic settings for hydrocarbon exploration (McKenzie, 1972; Dewey and Şengör, 1979; Le Pichon *et al.*, 1981; Şengör *et al.*, 1985; Taymaz *et al.*, 1991; Ilkişik, 1995; Ates *et al.*, 2012). The discovery of the Prinos oil field in the northern Aegean Sea (Proedrou and Sidiropoulos, 1992) and the discovery of gas in the Thrace Basin (Perincek, 1991; Huvaz *et al.*, 2005; Siyako and Huvaz, 2007) has encouraged the Turkish National Petroleum Corporation (TPAO) to investigate Neogene grabens in western Anatolia. These include the east-west trending Saros (SaG), Edremit (EG), Gediz (GG), Büyük Menderes (BMG), Küçük Menderes (KMG) and Gökova (GöG) grabens and the north-south trending Bakırçay (BçG), Denizli (DG) and Simav (SG) grabens (Fig. 1). These grabens have a non-marine stratigraphic fill (lacustine, alluvial and fluvial) which also includes the products of Neogene volcanism. The Küçükkuyu Formation of the Edremit graben (Çiftçi *et al.*, 2004) and the Soma Formation of the Bakırçay graben (Yılmaz *et al.*, 2000) constitute potential lacustrine source rocks.

However in general, depocentres are 1500 to 3000 m in thickness (Çiftçi *et al.*, 2010) and burial may not be sufficient for source-rock maturation. Intense Neogene volcanism and associated hydrothermal circulation may help to overcome this problem by providing local sources of heat input. Geothermally induced hydrocarbon generation may occur at the intersection of east-west and NE-SW trending grabens (such as the Büyük Menderes and Denizli grabens: Gürgey *et al.*, 2007). Surface oil seeps have been observed (Fig. 1) in the Edremit and Bakırçay grabens implying the presence of mature source rocks despite the relatively thin sedimentary successions (~1000 m, Yılmaz *et al.*, 2000). The neighbouring Gulf of İzmir has a similar geological background to the Bakırçay and Edremit grabens, but no hydrocarbons have been found here and the offshore Foça-1 well (location in Fig. 1b) proved to be dry (Çiftçi *et al.*, 2010).

In this context, this paper reports on the hydrocarbon potential of the part of the Gulf of İzmir where the east-west oriented Gediz and NE-SW oriented Bakırçay grabens intersect. Significant hydrothermal circulation is reported here due to Neogene volcanic activity (Ilkişik, 1995; Düşünür-Doğan and Üner, 2019).

A major challenge in the study area is concerned with the imaging and interpretation of igneous rocks. The methodology used in this study is based on seismic methods which are well suited to the detection of amplitude anomalies (direct hydrocarbon indicators such as bright spots, flat spots, dim spots and polarity reversals). However, it is often not clear whether an amplitude anomaly is in fact due to the presence of hydrocarbons. High-porosity wet sands (23% of all prospects) or low-saturation gas sands (11% of all prospects) are the most common reasons for the failure of DHI-located prospects (Forrest *et al.*, 2010). The identification of individual DHIs on seismic profiles may be unsatisfactory, but the presence of multiple indicators may point to the presence of a prospect.

The methodology also includes reflection tomography (Bishop *et al.,* 1985). Velocity model building by reflection tomography for pre-stack depth migration has become a standard tool in the oil and gas industry.

Time migration does not produce images which reliably represent the geology of the subsurface, especially in areas with complex structural geology in which there are lateral velocity variations, as occur in the present study area (Taner and Baysal, 1993). Images in the depth domain or in the pre-stack are more reliable to interpret. Image analyses was therefore carried out in the depth domain, in contrast to previous investigations which were carried out in the time domain. Stratigraphic information came from the offshore Foça-1 well in the Gulf of İzmir (Fig. 2). Seismic data came from a 27 km long, NW-SE oriented profile in the outer part of the Gulf (Fig. 1b). Reflection tomography, pre-stack depth migration, seismic modelling and seismic attribute analysis were used to identify possible low-velocity zones and hydrocarbon-saturated intervals.

Tectonic and Geological Setting

The Anatolian microplate is at present escaping to the west (Fig. 1a), with counter-clockwise rotational motion taken up along the dextral North Anatolian Fault (NAF) and sinistral East Anatolian Fault (EAF). Subduction of the African Plate beneath Anatolia (through the Hellenic arc) has resulted in north-south extension (McKenzie, 1972; Dewey and Şengör, 1979; Le Pichon *et al.*, 1981; Şengör *et al.*, 1985; Taymaz *et al.*, 1991) at a rate of 30 to 40 mm/yr (Le Pichon *et al.*, 1995) in western Anatolia (Fig. 1a). Extension in the region is characterized by crustal thinning (Ates *et al.*, 2012), seismic activity (Taymaz *et al.*, 1991; Reilinger *et al.*, 1997), and high heat flows associated with volcanism (Ilkişik, 1995; Yılmaz *et al.*, 2001; Tokçaer *et al.*, 2005; Bilim *et al.*, 2016) and geothermal activity (Tarcan *et al.*, 2005; Altan and Ocakoğlu, 2016; Üner *et al.*, 2019). The ongoing extension has created numerous east-west trending (and less common north-south trending) Neogene grabens and horst blocks in western Anatolia (Fig. 1a). The horst-graben geometry together with the volcanic activity and elevated heat

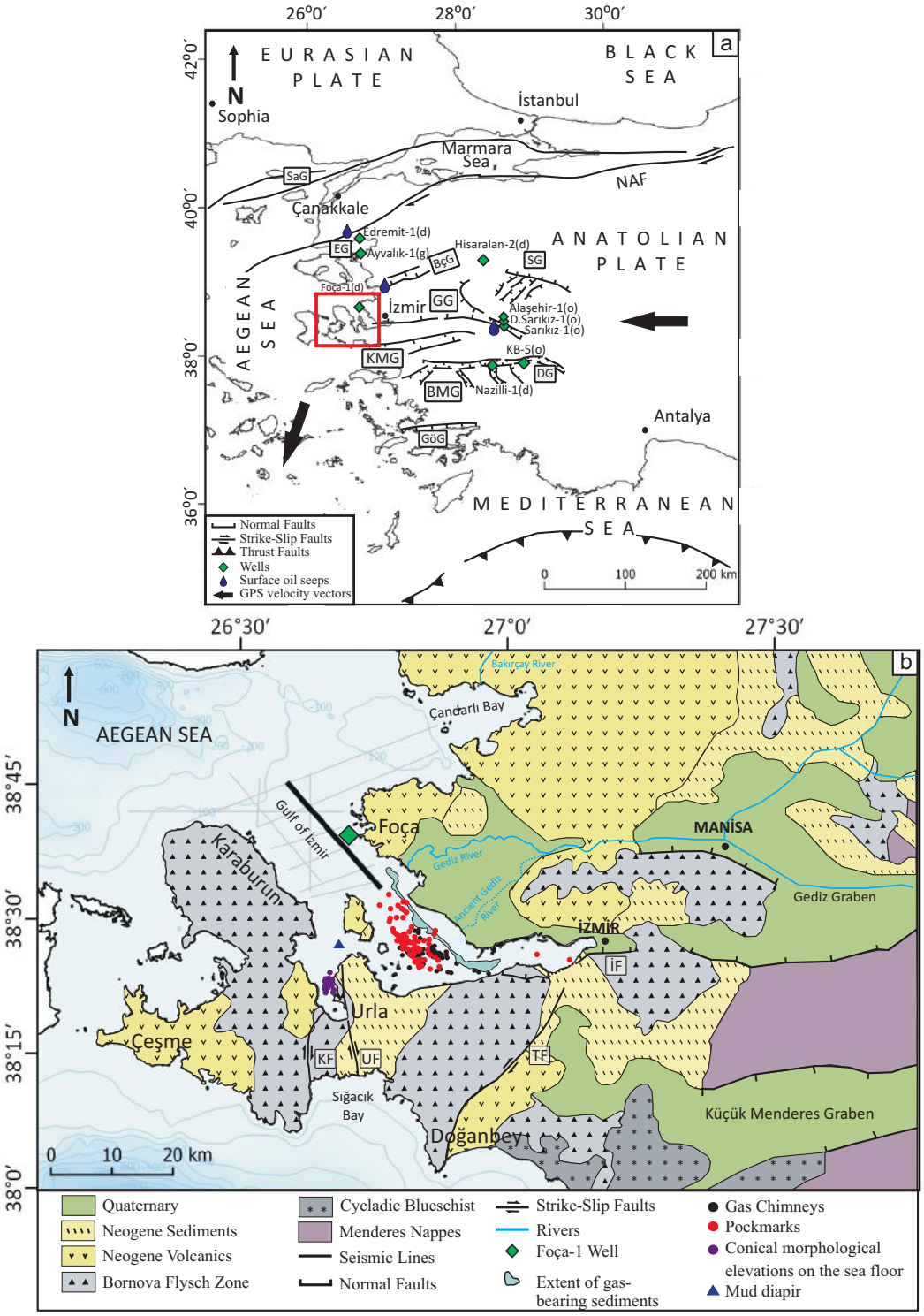

Fig. 1. (a) Location map of western Anatolia showing the study area (red square box) together with the main tectonic elements and major grabens (compiled from Şengör *et al.*, 1985; Taymaz *et al.*, 1991; Şaroğlu *et al.*, 1992; Reilinger *et al.*, 1997; McClusky *et al.*, 2000; Imren *et al.*, 2001; Ustaömer *et al.*, 2008). Offshore and onshore wells (green diamonds) and the locations of surface oil seeps (blue drops) are compiled from Çiftçi *et al.* (2010). Abbreviations: NAF = North Anatolian Fault; SaG = Saros Graben; EG = Edremit Graben; BçG = Bakırçay Graben; SG = Simav Graben; GG = Gediz Graben; KMG = Küçük Menderes Graben; BMG = Büyük Menderes Graben; DG = Denizli Graben; GöG = Gökova Graben; o = Wells with oil; g = Wells with gas; d = Wells without oil/gas (dry). (b) Geological map of the study area (after the 1:100,000 scale geological map of Turkey, map sheets K16-18 and L16-18). Onshore active faults (black solid lines) are adapted from Şaroğlu *et al.* (1992), Emre *et al.* (2005) and Genç *et al.* (2001). The offshore extent of gas-bearing sediments, gas chimneys and pockmarks are derived from Dondurur *et al.* (2011); mud diapir from Altan and Ocakoğlu (2016); conical sea-floor elevations (due to clustering of corals around hydrothermal vents) from Pekçetinöz (2010). Abbreviations: KF = Karaburun Fault; UF = Urla Fault; TF = Tuzla Fault; IF = Izmir Fault.

flows (average 107±45 mWm^{-2} in western Anatolia: Ilkişik, 1995) make this region attractive for both geothermal and hydrocarbon exploration. Onshore studies have investigated the region's geothermal (Filiz and Tarcan, 1993; Drahor and Berge, 2006; Aksoy *et al.*, 2008; Pamukçu *et al.*, 2014; Bilim *et al.*, 2016) and hydrocarbon potential (Perincek, 1991; Çiftçi *et al.*, 2004, 2010).

Hydrocarbon exploration in western Anatolia began in the 1970s and a comprehensive review of hydrocarbon occurrences in the area was presented by Çiftçi *et al.* (2010). Two offshore wells (Edremit-1 and Foça-1) and numerous onshore wells (including Ayvalık-1, Hisaralan-2, Alaşehir-1, D. Sarıkız-1, Sarıkız-1, Nazilli-1 and KB-5 in Fig. 1a) were drilled by TPAO until the 1990s. The exploration results were in general not encouraging until well Alaşehir-1 was drilled in the Gediz graben; this well suggested the presence of good-quality oil (Çiftçi *et al.*, 2010).

Geomorphologically, the Gulf of İzmir (Fig 1b) is composed of an east-west oriented inner bay extending from İzmir city to Urla, and a NNW-SSE oriented outer bay between offshore Foça and Karaburun. It is bound by the Gediz Delta to the east and the Karaburun Peninsula on the west. The study area is covered by Neogene sediments and volcanics, the latter cropping out around Foça, on Hekim Island and at the south of the Karaburun Peninsula; Quaternary alluvium dominates the Gediz delta. The Late Cretaceous Bornova Flysch is exposed in the central Karaburun Peninsula and between İzmir and Doğanbey (Fig. 1b). Prominent north-south trending strike-slip faults include the Karaburun (KF), Urla (UF) and Tuzla faults (TF) (Fig. 1b); east-west trending normal faults include the İzmir fault (İF, Fig. 1b). These faults extend offshore into the Gulf (Aksu *et al.*, 1987; Ocakoğlu *et al.*, 2005; Altan and Ocakoğlu, 2016).

The Foça-1 well (TD ~2100 m) is located in the outer bay area of the Gulf of İzmir (Fig. 1b) and five lithostratigraphic formations have been defined here (Fig. 2). At the base is the lacustrine lower-middle Miocene Soma Formation which is overlain by the thick Yuntdağ Volcanics with lacustrine limestone intervals. Yılmaz *et al.* (2000) and Çiftçi *et al.* (2010) noted that organic-rich shales in the Soma Formation in the Bakırçay graben may have source rock potential (Fig. 2, upper right-hand corner). Minor sandstones and tuffs in the Yuntdağ Volcanics may have reservoir potential, and tight volcanic facies may be considered as seals.

Upper Miocene alluvial-fluvial sandstones, limestones, volcanics and shales of the Bozköy Formation rest unconformably on this succession. Above are lacustrine limestones of the Pliocene Ularca Formation which are unconformably overlain by the Quaternary Bayramiç Formation.

Even though no hydrocarbons were reported in the Foça-1 well, a number of seismic features were observed which could be interpreted as possible indications of gas leakage or fluid discharge. Geophysical evidence for fluid discharge (Pekçetinöz, 2010; Kayseri-Özer *et al.*, 2014) and subsurface gas-associated structures such as gas chimneys, pockmarks, mud diapirs and acoustic turbidity zones (Dondurur *et al.*, 2011; Altan and Ocakoğlu, 2016; Coskun *et al.*, 2016) have been detected by single-channel seismic reflection studies and acoustic methods in the inner and outer parts of the Gulf of İzmir. These observations together with the results of previous studies justify further study of the region.

DATA AND METHODOLOGY

The seismic dataset used in this study was acquired during the summer of 2000 onboard the R/V Sismik-1 which is owned and operated by the Turkish General Directorate of Mineral Research and Exploration (MTA). The Sismik-1 was configured to have 6 km streamers with a receiver spacing of 12.5 m. The streamers were towed at a depth of 10 m with a total of 48 channels, and sources were made up of six GI airguns with a total capacity of 780 cu. in. The airguns were towed at a depth of 10 m and fired every 25 m. The total recording window was 3 s. These parameters provided 12 common-depth-point (CDP) data.

Reflection Tomography

Travel-time picking

Reflection tomography is an inversion method widely used to determine velocity distributions and reflector depths (Stork, 1992). The key factors affecting the tomographic inversion procedure are the interpretation of, and travel time extraction from, pre-stack data. Travel times are digitized across horizons on pre-stack time sections (Bording *et al.*, 1987), and the inversion quality mostly depends on the quality of the original data. Due to the excessive background noise in the pre-stack data in this study, some pre-processing steps were required such as editing, notch filtering and trapezoidal band-pass filtering (*see data-processing flow chart in Appendix Fig. 1: page 224*) to distinguish hyperbolas for travel-time picking.

A post-stack time-migrated 2D seismic line (~27 km long), previously processed by Ocakoğlu *et al.* (2005), was re-interpreted in terms of changes in reflection configurations, reflection terminations, and unconformity surfaces before applying the tomographic scheme (see line location in Fig. 1b). Five seismic stratigraphic units/sub-units (from the base up: SSU3, SSU2, and SSU1c, b and a) were distinguished and are bounded above and/or below by horizons H5-H1 (Fig. 3).

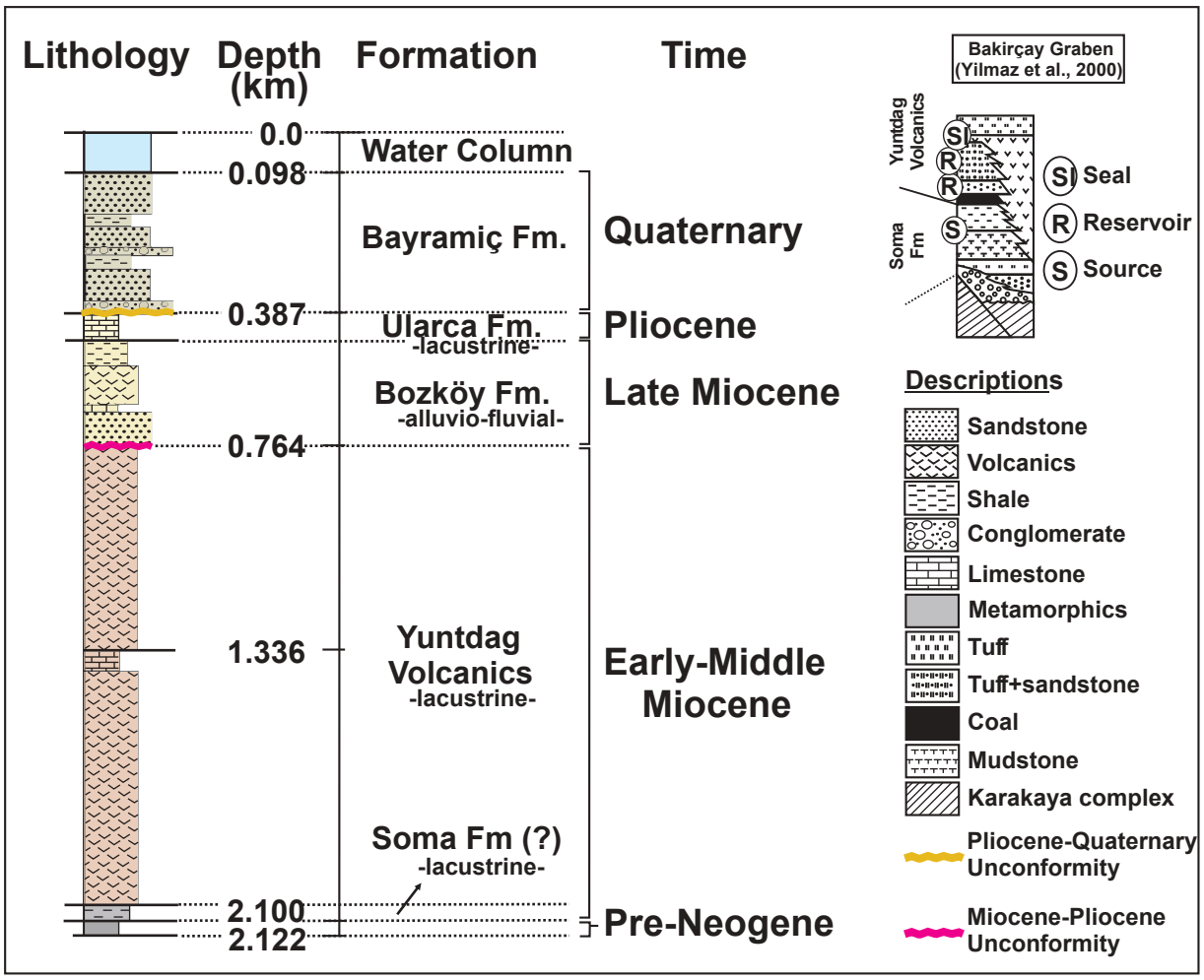

Fig. 2. Stratigraphic nomenclature for the Foça-1 well in the Gulf of Izmir (location in Fig. 1b). Formation names, time-scale and depositional environments are adapted from Yılmaz *et al.* (2000) and Çiftçi *et al.* (2010). Source, reservoir and seal potential of the Yuntdağ Volcanics and Soma Formation in the adjacent Bakırçay graben are shown in the cartoon in the upper right-hand corner. Note that the Yuntdağ Volcanics and Soma Formation are also present in the Foça-1 well.

The H5 horizon was picked on the pre-stack time section as a high-amplitude reflection indicating an erosional surface. It bounds the top of the acoustic basement (SSU3) which is characterized by chaotic reflections (Box III in Fig. 3). Next, horizon H4 was picked as an unconformity which terminates the thickest sedimentary package (SSU2). This package has a discontinuous, low-frequency reflection character with low amplitude reflections onlapping onto horizon H5 (Box III in Fig. 3b). SSU2 is overlain by SSU1c which shows continuous, low frequencies with low-medium amplitudes and with top-laps at the upper surface (H3; Box II, Fig. 3b). Horizon H2 was traced bounding the top of SSU1b which has continuous and low-frequency reflections exhibiting medium-high amplitudes (Fig. 3b). SSU1b is overlain by SSU1a which is represented by a parallel reflection pattern constituting an onlap onto the H2 horizon at the SE tip of the seismic line (box I in Fig. 3b). Finally, horizon H1 was picked at the top of SSU1a which constitutes the seafloor (Fig. 3a).

1.2 Ray tracing and Tomographic Inversion

The tomographic software CAT3D, developed by the Istituto Nazionale di Oceanografia e Geofisica Sperimentale (OGS) based on minimum-time ray tracing (Böhm *et al.*, 1999), and the simultaneous reconstruction technique (SIRT) developed by Stewart (1991), were used to invert the picked reflected travel times. In this scheme, the reflected travel times picked on the pre-stack data were first inverted; then the velocity field and the seismic stratigraphic unit structure in depth were estimated sequentially by following a layer-stripping approach. An iterative procedure starting from constant velocity within the seismic unit and a horizontally flat interface (or uniform thickness) was used for each horizon.

Twenty-seven quadrangular grids were chosen to define the velocities in the initial model for tomographic inversion. This grid corresponds to a sampling interval of 1 km. The picked travel times were inverted, and the velocity model updated in each iteration. Then the new interface was estimated by following the principle

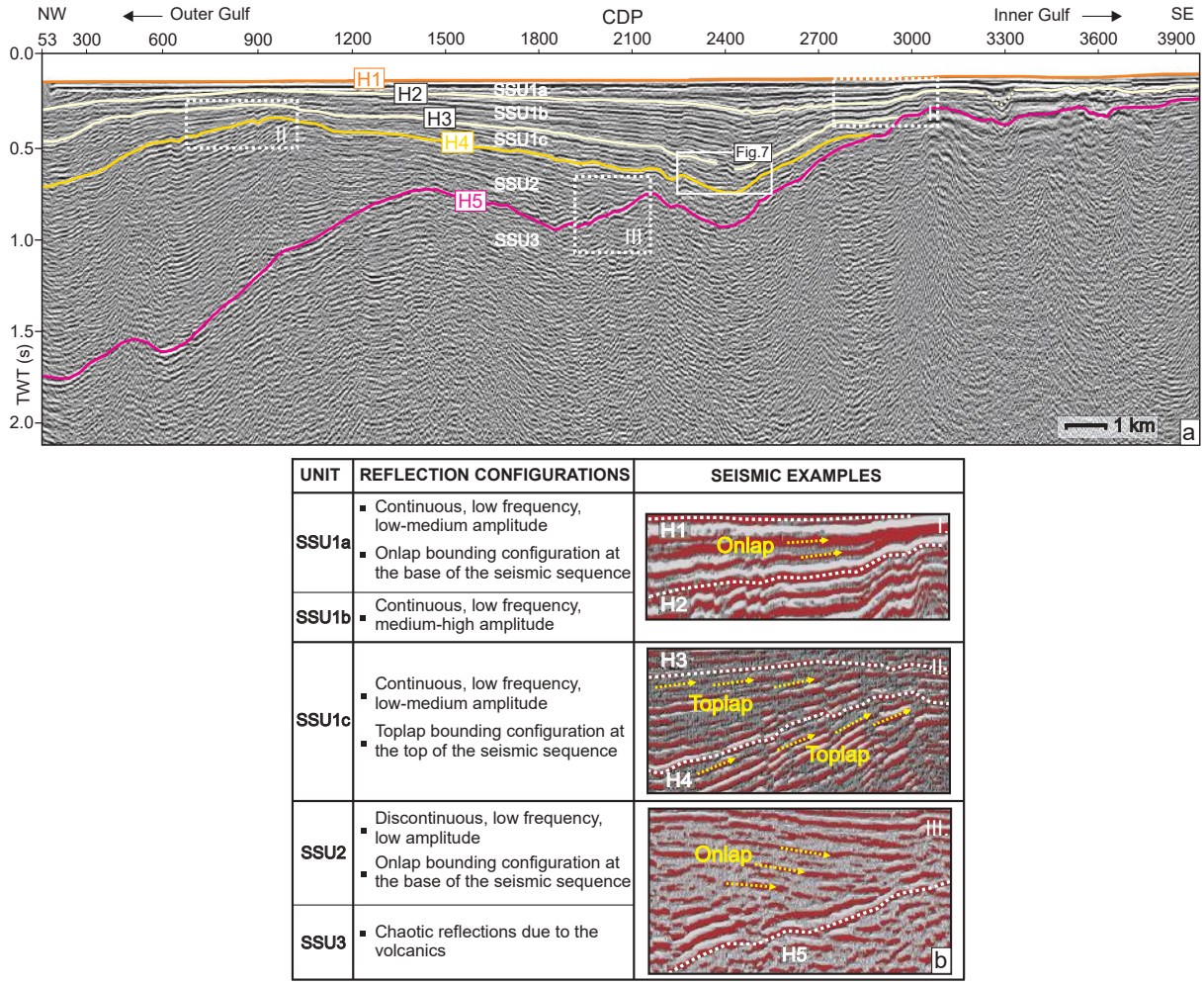

UNIT	REFLECTION CONFIGURATIONS	SEISMIC EXAMPLES
SSU1a	▪ Continuous, low frequency, low-medium amplitude ▪ Onlap bounding configuration at the base of the seismic sequence	
SSU1b	▪ Continuous, low frequency, medium-high amplitude	
SSU1c	▪ Continuous, low frequency, low-medium amplitude ▪ Toplap bounding configuration at the top of the seismic sequence	
SSU2	▪ Discontinuous, low frequency, low amplitude ▪ Onlap bounding configuration at the base of the seismic sequence	
SSU3	▪ Chaotic reflections due to the volcanics	

Fig. 3. Re-interpreted time-migrated NW-SE oriented seismic section from the offshore Gulf of Izmir (profile location in Fig. 1b) (adapted from Ocakoğlu *et al.*, 2005). Two sedimentary units (SSU1 and SSU2) together with acoustic basement (SSU3) are distinguished; SSU1 is divided into the SSU1a, SSU1b and SSU1c sub-units. These units are bordered by reflection horizons H1-H5 represented by orange, beige, yellow and pink colours, respectively. Toplap/onlap reflection terminations used in the interpretation phase to mark the main unconformities are shown in the white dashed-line boxes. Reflection configurations associated with the sedimentary units are listed in the table below the section.

of minimum dispersion of the reflected points (Carrion *et al.*, 1993). The velocity field updated in the first step of any iteration was used for depth conversion of the travel time residual associated with each reflected event. In the inversion procedure, the "staggered grid" method was used (Vesnaver and Böhm, 2000) and two new grids were created by shifting the initial grid 0.33 and 0.66 km (one-third of the sampling interval) along the line direction. Tomographic inversion was then carried out using the initial grid and the new shifted grids, obtaining the final estimated velocities averaged in the points of a high-resolution grid and resulting in a high-resolution final image (Fig. 4).

Depth Migration

In this study, post- and pre-stack depth migrations (PostSDM and PreSDM, respectively) were carried out. For the PostSDM, Omega-X Finite Difference Migration (Kjartansson, 1979; Claerbout, 1985) was used; and for PreSDM, a standard Kirchhoff depth migration was performed using Echos software and SeismicUnix code (Cohen and Stockwell, 2003).

Depth migration is dependent on an accurate velocity-depth model. To overcome this dependency, a velocity model reproduced via iterative tomographic analysis was used to carry out both post- and pre-stack depth migration. The final products of both depth migrations were compared and evaluated (Fig. 5). It was also used for correlation of the seismic stratigraphic units interpreted in this study with the results of the Foça-1 well (Fig. 6).

AVO Analysis

The AVO analysis was applied to CDP gathers of the real data to check whether amplitude variations with offset changes occur at the levels of interest. Reflections usually tend to decrease in amplitude with offset, but anomalous reflections may indicate

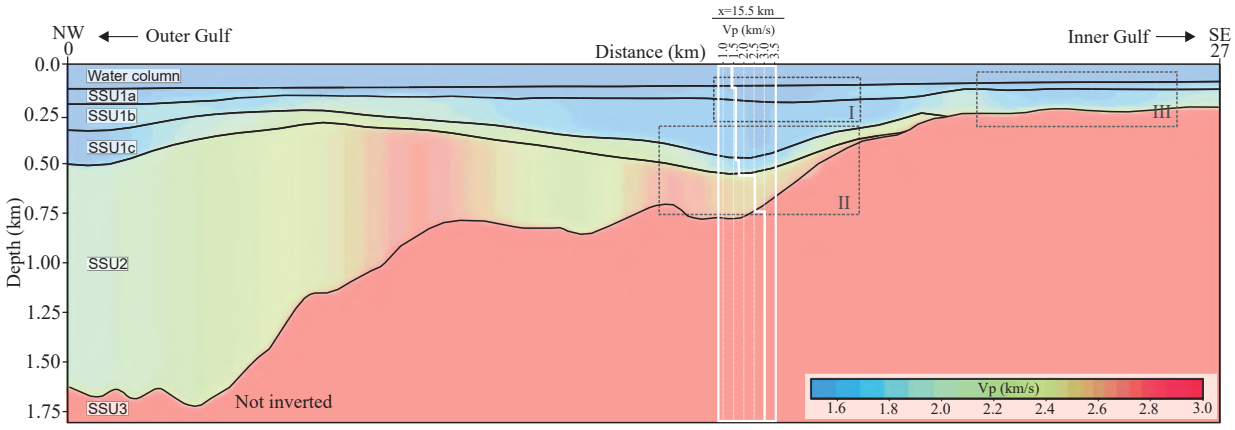

Fig. 4. 2D seismic velocity model for the studied profile derived from the travel times of the picked horizons in Fig. 3. A vertical 1D velocity function overlapped on the velocity-depth section indicates a number of laterally-varying low velocity zones (shown in boxes I, II and III). Four sedimentary units (SSU1a, SSU1b, SSU1c and SSU2) plus basement (SSU3) were identified; however, SSU3 was not inverted.

the presence of pore fluids. The AVO analysis can help to discriminate amplitude effects due to rock matrix variations from those due to the presence of fluids (Rutherford and Williams, 1989). AVO analysis requires a processing work-flow where the amplitudes are preserved (Castagna, 1993). For this, trace-by-trace amplitude scaling was not used but a spherical divergence correction was applied. NMO-corrected, pre-stack CDP gathers with true amplitude preserved were used to examine AVO plots (Fig. 7).

Seismic Modelling

The synthetic seismic section was generated for the possible DHIs and accompanying structure in order to confirm the seismic response of the interval velocities which obtained in the tomographic analysis, and to ascertain the characteristics of the amplitude anomalies.

The modelling approach used was based on the interval velocity at the horizon point (V), and depth of the horizon point (Z), produced by reflection tomography. Four steps were followed: (i) the acquisition array and subsurface geometry were defined; (ii) velocity and depth information of the formations extracted from the tomographic analysis were described to the database; (iii) normal incidence ray tracing was performed to obtain the synthetic data; (iv) finally, a low-pass of a zero-phase Hamming filter with corner frequencies 90-160 Hz was applied to the seismic response. The response model consists of only primary reflection coefficients (Fig. 8c).

Seismic Attribute Analysis

In this study, a combination of several post-stack attributes was adopted to reduce uncertainty and risk, and to improve the interpretation of possible DHIs (Fig. 8). Minimally processed data were used for the extraction of the attributes from the seismic data to maintain the effects of natural phenomena, as opposed to artefacts caused by processing. Reflection strength, instantaneous frequency and instantaneous phase were derived to isolate high or low amplitude areas associated with bright/flat/dim spots, to indicate hydrocarbons in terms of low-frequency anomalies, and to discriminate geometrical shapes and the lateral continuity of the formations, respectively. In addition, relative acoustic impedance was extracted from the seismic data, providing information about how impedance changes in a relative sense.

RESULTS

The velocity-depth model generated by the reflection tomography for the acoustic basement (SSU3) displays a basin-and-ridge morphology which is detailed to a depth of 1.8 km in the study area (Fig. 4). The top-acoustic basement (SSU3) deepens from a depth of ~230 m below the ocean surface in the SE of the studied profile, to ~780 m in the centre, and then ~1720 m in the NW of the profile in the outer part of the Gulf of Izmir (Fig. 4). The thickest of the overlying sedimentary packages is SSU2 which is ~1320 m thick in the NW of profile, thinning to ~60 m to the SE where it onlaps the basement (Fig. 4 and Table 1). This unit is overlain by the thinner SSU1c unit, whose depositional geometry mimics the upper surface morphology of SSU2 (Fig. 4); SSU1c rests on SSU3 to the SE (Fig. 4). It is overlain by a relatively thicker unit, SSU1b (~125 m thick), which rests on acoustic basement in the far SE (Fig. 4). SSU1b reaches a maximum depth (~350 m) in the centre of the profile in Fig. 4. Above this unit, SSU1a has an average thickness of 58 m, and is overlain by the water column whose thickness changes from 106 m in the NW to 70 m in the SE (Fig. 4 and Table 1).

Reflection tomography shows an increasing interval P-wave velocity (Vp) trend with depth associated with

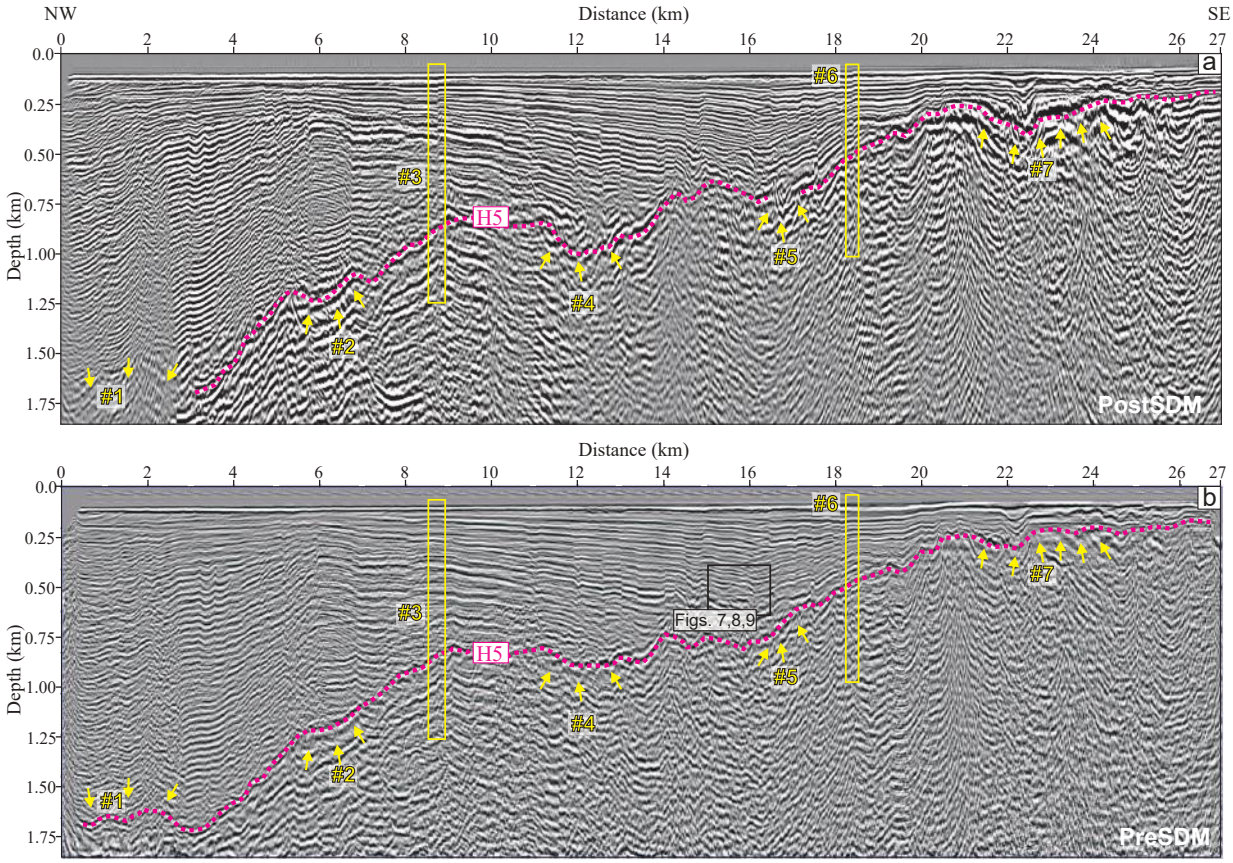

Fig. 5. Comparision of the final products of different depth-migration approaches derived from the 2D velocity-depth model produced by the tomographic inversion. (a) Post-stack depth migration; (b) pre-stack depth migration. Line location in Fig. 1b. Black rectangle represents the lenticular structure with direct hydrocarbon indicators (see text for details).

each seismic unit (from 1.5 km/s to 2.7 km/s; Fig. 4, Table 1). In addition, Vp-values show lateral variations within units SSU1a, SSU1b and SSU1c (Fig. 4, dashed boxes I, II, III). Within this framework, an area was recognized which has particularly low velocity values compared to the surrounding rocks. According to the 1D interval velocity function from the final tomography result, the velocity of SSU1a varies between 1.5 km/s and 1.73 km/s from NW to SE, and it is 1.52 km/s at x = 15.5 km. It increases to 1.58 km/s within SSU1b and is 1.7 km/s in the surrounding rocks. This trend continues within SSU1c with a velocity of 1.68 km/s. However, the surrounding rock has increased velocities (~2.2 km/s) on both sides of this low-velocity zone (Fig. 4). The LVZ occurs around 15 km to the SE of the the centre of the profile. It overlaps a lenticular structure in the time-migrated seismic section between 0.60 and 0.72 s (solid white rectangle in Fig. 3).

The velocity function increases significantly in the underlying unit SSU2 (Fig. 4). The velocity of the surrounding rocks increases from 2.6 km/s to 2.8 km/s (box II in Fig. 4). Another LVZ (box III in Fig. 4 in the SE of the profile) can be seen in the sediments within sub-units SSU1a and SSU1b deposited over the acoustic basement. The velocities in this zone range between 1.61-1.63 km/s. To interpret the lenticular structure and the surrounding sediments, the time-migrated section was converted to the depth domain (Fig. 5) using the velocity model displayed in Fig. 4.

There is an acceptable degree of similarity between the Post- and PreSDM sections in Figs 5a and b. This is particularly true for the deposits which rest on top of acoustic basement. However, the signal-to-noise ratio was improved more in the PreSDM than in the PostSDM section.

There is less similarity in two sections for the upper surface of the acoustic basement (horizon H5, pink solid line in Fig. 5). The resolution of H5 at the lower-left corner of the section does not appear clearly on the PostSDM section (represented by Event #1 in Fig 5a) but it can be followed easily on the PreSDM section (Fig. 5b). U-shaped segments of H5 (e.g. Events #2, #4, #5 and #7 in Figs 5a and 5b) which are clear on the PostSDM section are not so easily visible on the PreSDM section. Instead, they have moved to their true subsurface positions; thus, errors in the interpretation were minimised.

The faults traced by vertical offsets along the reflection horizons were more clearly imaged on the PreSDM section. Possible fault traces on the PostSDM

Table 1. Velocities and layer thicknesses for the stratigraphic units interpreted in this study. The oldest layer is displayed at the bottom and the youngest at the top. Layer thicknesses are showed in terms of time and depth.

Layers	Lithologies	Min. Velocity (m/s)	Max. Velocity (m/s)	Min. Thickness		Max. Thickness	
				Time (ms)	Depth (m)	Time (ms)	Depth (m)
Water Column	-	1404	1500	122	70	142	106
SSU1a	Sandstone	1504	1734	24	30	176	86
SSU1b	Shale, sandstone and conglomerate	1584	1957	86	76	310	298
SSU1c	Shale, sandstone and conglomerate	1687	2342	70	61	122	176
SSU2	Limestone, shale, volcanics, limestone and sandstone	2022	2722	40	60	1242	1321

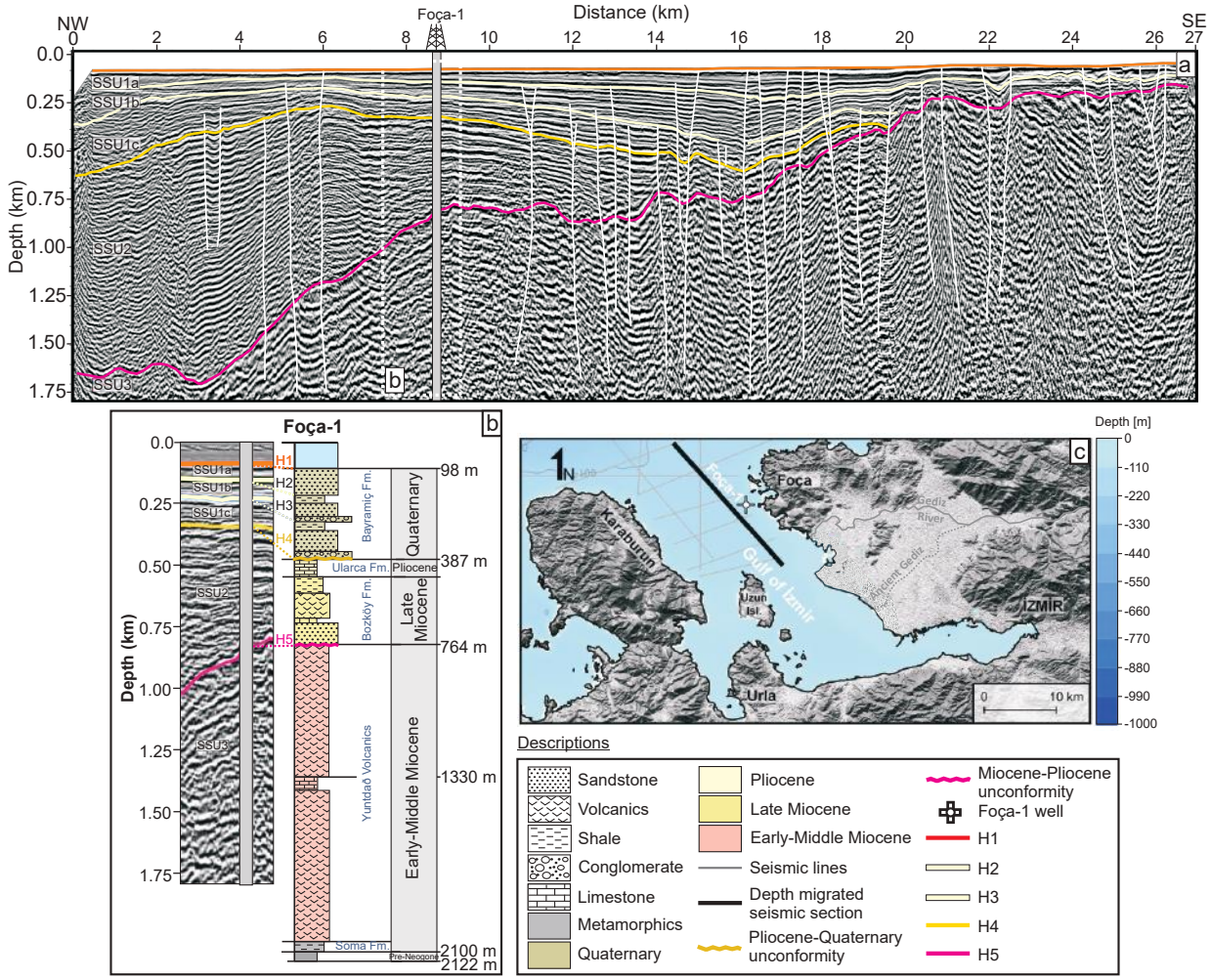

Fig. 6. (a) Structural and stratigraphic interpretations shown on the depth-migrated section. Interpreted geological horizons are plotted as orange, beige, yellow and pink solid lines. The location of the Foça-1 well is projected onto the PreSDM section. Strike-slip faults cutting through the entire section are represented by solid white lines. (b) Correlation of the various formations identified at the Foça-1 well with the depth-migrated section. Interpreted horizons (H5-H1) in the study area corresponds to the boundaries of units and sub-units. (c) Map showing the location of the 2D line in the study area.

section were seen as an artefacts on the PreSDM (compare Events #3 and #6 in Figs 5a, 5b; see Fig. 6a for the location of the faults).

The stratigraphic units and structural elements were interpreted on the pre-stack depth-migrated section (Fig. 6a), since the PreSDM process improved the resolution of the seismic data. The Foça-1 well was tied with the PreSDM section (Fig. 6b). The acoustic basement associated with SSU3 in the depth-migrated section is likely tied to the Lower-Middle Miocene Yuntdağ Volcanics consisting of tuffs, sandstones, limestones and volcanics between depths of 764 and 1750 m (Fig. 6b). The top of SSU3 (horizon H5) is marked as a major unconformity in the depth section at about ~760 m and is well correlated with the Upper Miocene unconformity within the Yuntdağ Volcanics at ~764 m. The first rocks deposited on top of acoustic basement (SSU2) correspond to the sandstones,

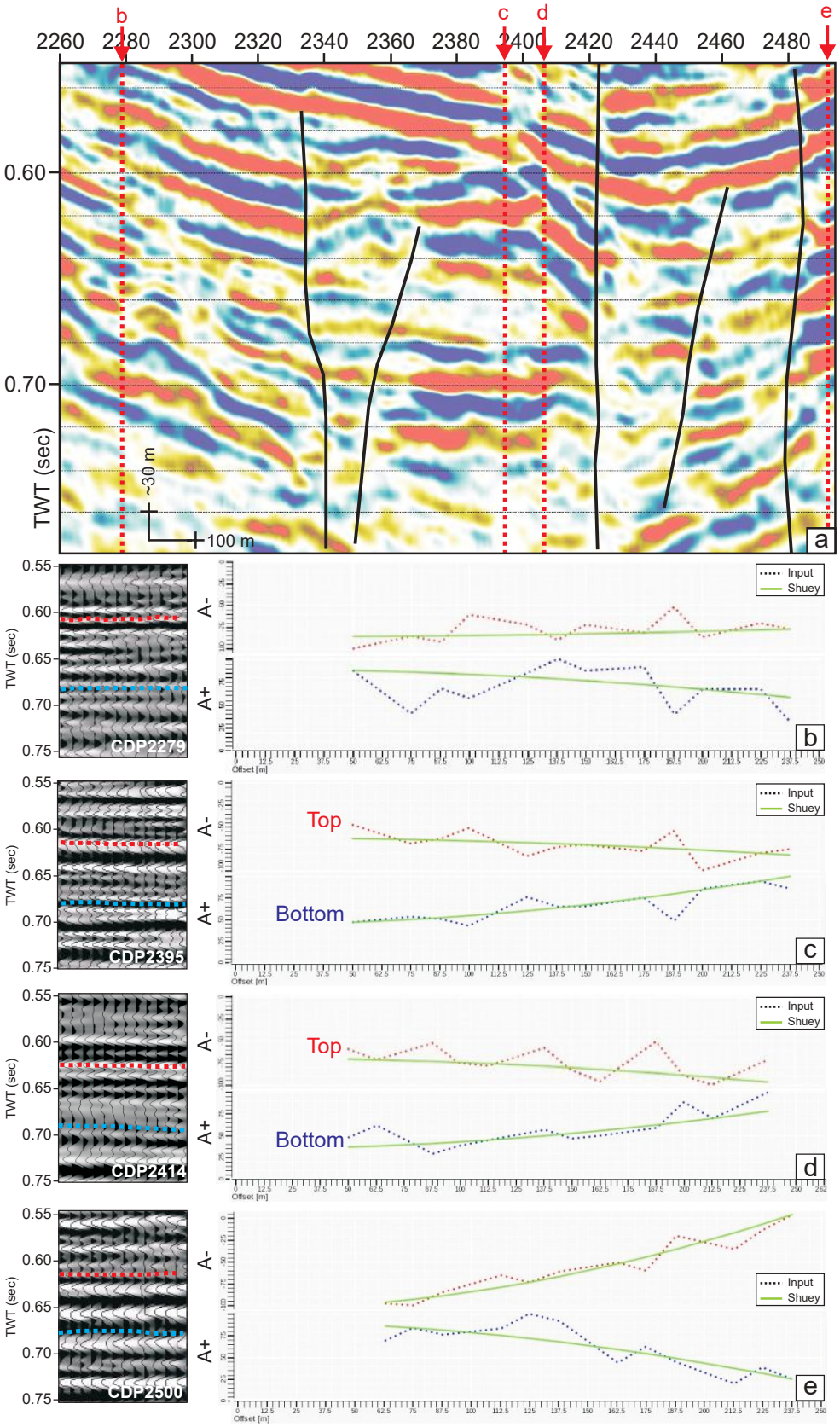

Fig. 7. (a) Section of the studied seismic profile indicating the lenticular structure which is bounded by strike-slip faults (represented by black solid lines) at both margins. See location in Fig. 5.
(b), (c), (d) and (e) Selected NMO-corrected CDP gathers (left-hand side) and AVO curves for relevant top and bottom amplitudes (right-hand side). Note that CDP 2395 and CDP 2414 indicate amplitude increases with offset for the top (red dashed line) and bottom (blue dashed line) reflections (positive standard polarity, with black representing a peak).

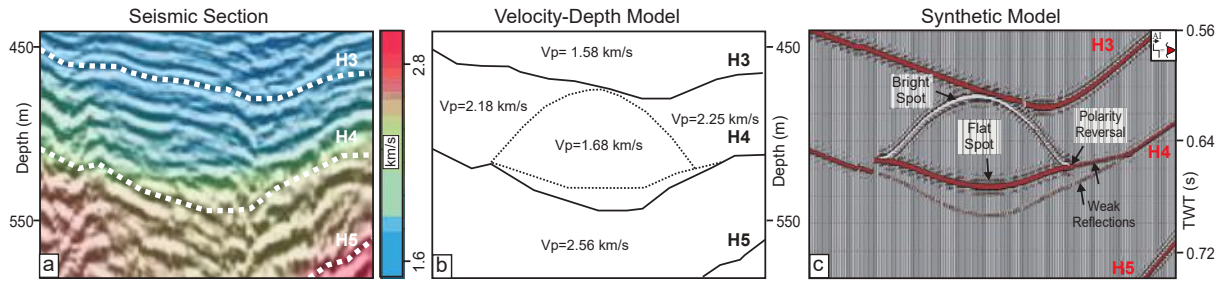

Fig. 8. 2D synthetic model generated to simulate the seismic data. (a) Velocity-depth model for the target zone; (b) model parameters; (c) synthetic gathers calculated from the velocity-depth model.

limestones, volcanics and shales of the Bozköy Formation and the limestones of the Ularca Formation between depths of 764 m and 387 m, dating from the Late Miocene to the Pliocene. The top of SSU2 (horizon H4) is interpreted as another unconformity in the depth section at about ~350 m and is correlated with the Pliocene unconformity at 387 m. Above that, part of the Bayramiç Formation (SSU1c) is dated as Quaternary, consisting of conglomerates at the base overlain by sandstones and shales above. On top of the SSU1c are two further sub-units of the Bayramiç Formation separated by horizons H3 and H2. SSU1b consists of a similar sequence of conglomerates, sandstones and shales; SSU1a consists of Quaternary sandstones.

The interpreted PreSDM section shows that the study area is deformed by numerous faults which cut through the seismic units and extend up to the seafloor (Fig. 6a).

The lenticular structure observed on the time-migrated section (Fig. 3) is present in the PreSDM section within the Bayramiç Formation (Fig. 5b, black rectangle). The structure is ~500 m long and ~90 m wide and is bounded by steeply-dipping faults on either side (Fig. 7a). Amplitude anomalies appear to be present at both the upper and lower surfaces of the structure in both time-migrated (white rectangle in Fig. 3) and depth-migrated (black rectangle in Fig. 5b) seismic sections.

AVO analyses were performed on selected CDP gathers in the area of the lenticular structure. For the CDP 2395 and CDP 2414 gathers at a depth of about 0.62 s at the top of the structure, there is a negative reflection whose amplitude increases with offset (Figs 7c and 7d, red dashed lines). The bottom reflector (at around 0.68 s) exhibits a positive reflection whose amplitude increases with offset (Figs 7c and 7d, blue dashed lines). However, the AVO curves calculated on the CDP 2279 and CDP 2500 gathers, which are outside of the lenticular structure, show reflections at the same levels of interest whose amplitudes in general decrease with offset (Figs 7b and 7e).

The synthetic seismic section of the lenticular structure (Fig. 8) shows results which are compatible with the observed data in terms of reflection character. A strong negative amplitude is observed at the top and a strong positive amplitude at the base. Polarity reversals at both the left- and right-hand margins of the structure are observed. Reflections beyond the fault zones bounding the structure and underlying it are relatively weak.

In the reflection strength section (Fig. 9a), there is a conspicuous vertical change from high reflection strength (light blue colour) in the upper part of the structure, to extremely low reflection strength (red-orange-yellow colour), and then high reflection strength again at the base of the structure. In a relative acoustic impedance section (Fig. 9b), polarity reversals have been detected at both sides of the structure. Low-frequency reflections (red to yellow colour) were recognised in the part of the instantaneous frequency section (Fig. 9c) where low amplitudes were observed in the reflection strength section (Fig. 9a). The lateral continuity of the reflectors in the instantaneous phase section (Fig. 9d) clearly indicates the boundary of the lenticular structure and the faults on each side.

DISCUSSION

Reflection tomography was carried out in this study to produce velocity-depth information, together with PreSDM, AVO analysis, seismic modelling and seismic attribute analysis. These multiple approaches were used to investigate the subsurface geology and hydrocarbon potential of a study area in the Gulf of İzmir.

The PreSDM section indicated the thickness of the Upper Miocene to Recent marine succession (~1750 m, SSU1-SSU3) which is present in the study area (Figs 5a and 6). The velocities observed throughout the velocity-depth model produced by the reflection tomography (Fig. 4) are consistent with average values, which are generally between 1.5-2.7 km/s for marine sedimentary rocks (Hamilton, 1978; Bourbié *et al.*, 1987).

Apart from the general velocity trend versus depth, three LVZs were observed. Of these, Areas I and III in Fig. 4, with P-wave velocities of 1.52 km/s and 1.63 km/s respectively, are interpreted as incoherent

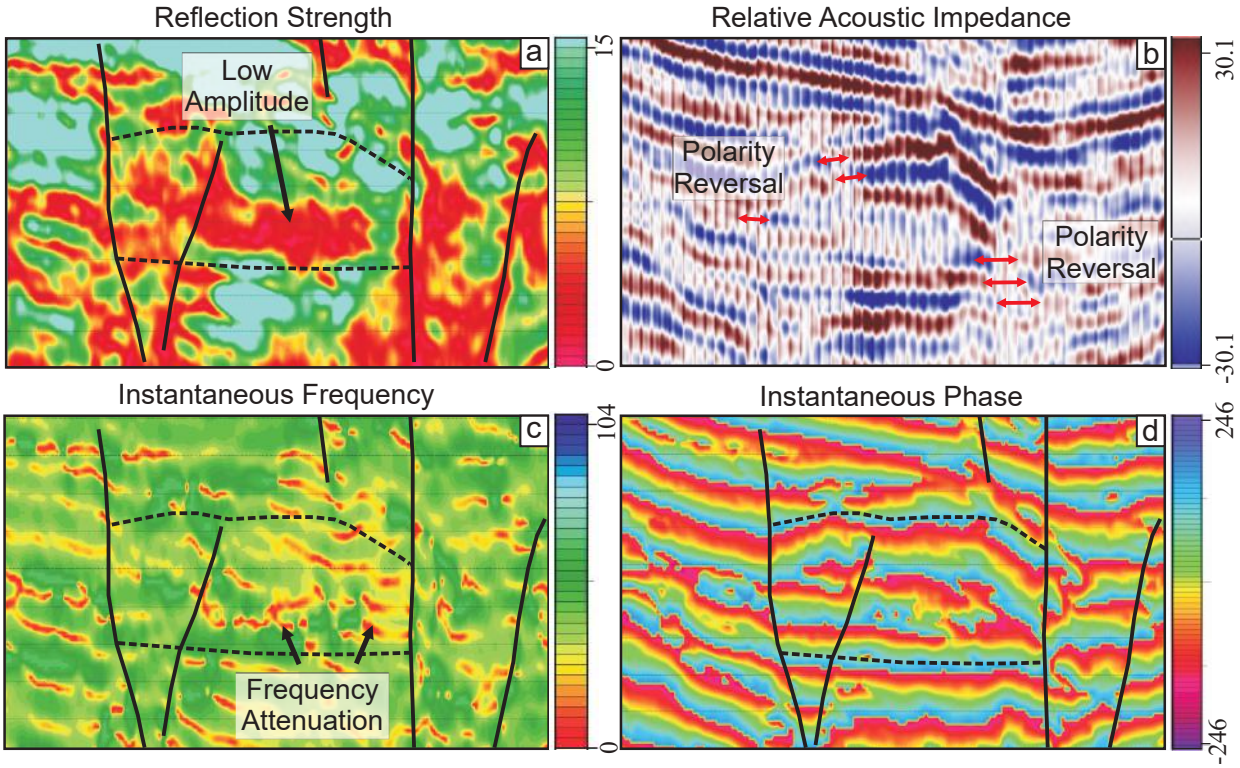

Fig. 9. Illustration of seismic attributes for the lenticular structure: (a) reflection strength, (b) relative acoustic impedance, (c) instantaneous frequency, and (d) instantaneous phase. Note how reflection strength emphasizes low amplitudes within the structure, and the instantaneous frequency section displays low-frequency reflections for the same zone. The relative acoustic impedance section shows negative impedance where there is a bright spot and positive impedance where there is a flat spot, together with polarity reversals at both margins of the structure. The instantaneous phase section shows vertical discontinuities at both margins of the structure. See Fig. 5 for the position of the sections displayed in this figure.

and uncompacted sediments corresponding to the Quaternary Bayramiç Formation which is composed of conglomerates, sandstones and shales. The presence of a possible buried valley in Area III indicates that sediment transport was supplied by the Gediz River in a high energy regime (Figs 4, 5 and 6a).

A significant lenticular-shaped structure was recognized in Area II within the Quaternary Bayramiç Formation and is buried to a depth of about ~500 m (Figs 4, 7, 8 and 9). This structure is characterized by low P-wave velocities (1.68 km/s) compared to the surrounding rocks (2.2 km/s) (Fig. 4). This abrupt lateral change in velocity may indicate the presence of hydrocarbons (particularly gas) in a porous formation (Taner and Sheriff, 1977; Simm *et al.*, 2014).

AVO analysis of the reflections at the top and bottom of the lenticular structure (Fig. 7) point to the presence of DHIs. Reflections with increasing negative amplitudes with offset are observed at the top of the lenticular structure, while positive reflections with increasing amplitude with offset occur at the bottom (Fig. 7c and 7d). These AVO trends could be evaluated to indicate the presence of as Class 2 gas sands within the Castagna (1993) classification scheme. Class 2 sands display little indication of gas on the near offsets; there is difficulty in distinguishing a clean wet sand from a gas sand due to the similar increasing behavior with offset. Although no far offset amplitude information is available due to the short receiver cable with which discriminate a gas sand from a wet sand, the amplitude increases at near offset point to a possible content of gas rather than water. Thus, the top DHI is interpreted as a bright spot while the bottom DHI as a flat spot.

The AVO analyses of reflections at these levels in CDP gathers outside the lenticular structure (Fig. 7b, e) show that amplitudes tend to decrease with offset. The structure may threfore be interpretd to represent a possible reservoir unit located within the Bayramiç Formation and consisting of conglomerates and sandstones. This localized zone is also apparent on the seismic attribute sections and can be correlated with the synthetic model (Figs 8 and 9).

Moreover, the lenticular structure with the DHIs at top and base is bounded by strike-slip faults on both sides (Fig. 7a). It is bounded at the base by an unconformity surface (horizon H4: Fig. 8) and above by the shales of the Bayramiç Formation, suggesting that the trap is not only structural but also has a stratigraphic component. The strike-slip faults cut through the entire cover succession and in general reach the seafloor (Figs 6, 7), and could allow the

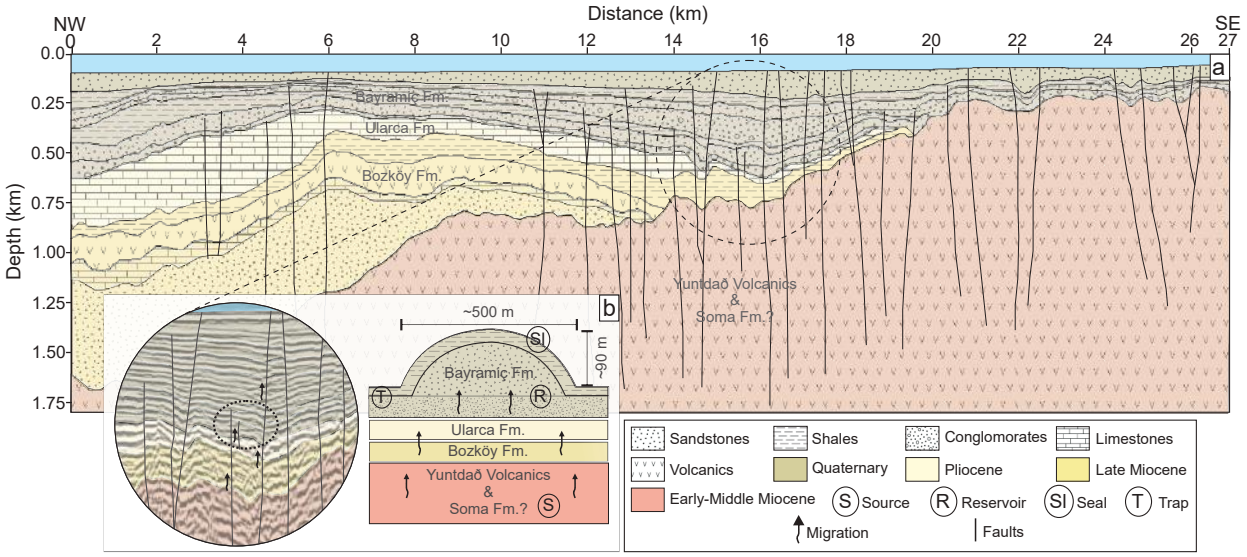

Fig. 10. (a) Schematic NW-SE oriented section showing the stratigraphy of the Gulf of Izmir. (b) (bottom left) Zoomed seismic section of the lenticular structure with hydrocarbon migration indicators. Strike-slip faults may provide conduits for the migration of hydrocarbons from lower to middle Miocene source rocks to the proposed structural-stratigraphic trap in the Bayramiç Formation. Cartoon (right) shows a model of the possible hydrocarbon system and trapping mechanism (combined structural-stratigraphic).

migration of hydrocarbons from source rocks located at greater depths (Fig. 10). The LVZs along these strike-slip faults (e.g. in Areas II and I: Figs 4, 7) could be evidence for upward gas leakage. The gas leakages and gas-associated structures observed in the study area by previous studies (Dondurur *et al.*, 2011; Altan and Ocakoğlu, 2016; Coskun *et al.*, 2016) are consistent with these general observations.

Potential hydrocarbon system

In the study area, conglomerates and sandstones of alluvial/fluvial origin are considered as potential reservoirs and are overlain by shales of the Bayramiç Formation (Fig. 10). This is consistent with hydrocarbon occurrences known elsewhere in western Anatolia which are mostly associated with sandstones overlying lacustrine shales and which are sealed by shales and mudstones (Çiftçi *et al.,* 2010).

In spite of the insufficient overburden for source rock maturation in the study area, it is thicker than that in the Bakırçay graben (~1000 m) where surface oil seeps have been reported (Fig. 1a) (Çiftçi *et al.*, 2010). Heat transfer from depth together with volcanism and geothermal activity may have led to thermal maturation of source rocks, as suggested by Gürgey *et al.* (2007) and Çiftçi *et al.* (2010). Heat transfer was mostly controlled by strike-slip faults in the study area, unlike grabens elsewhere in western Anatolia which have normal boundary and antithetic and synthetic faults (Fig. 10).

Yılmaz *et al.* (2000) and Çiftçi *et al.* (2010) noted that the Soma Formation in the adjacent Bakırçay graben comprises Lower to Middle Miocene lacustrine shales may have source rock potential. Although the Bakırçay graben and Gulf of İzmir have similar overall stratigraphies, it was not possible to locate the Soma Formation in the present study due to the limited depth of penetration (~1.75 km, Figs 6 and 10) and sporadic distribution of the formation.

The presence of gas in Plio-Quaternary sediments may be of commercial interest (c.f. Carstens, 2005), and the presence of a shallow, gas-saturated lenticular-shaped reservoir may point to the presence of other, deeper reservoirs (e.g. Heggland, 1998) in and around the Gulf of İzmir. The detection of DHIs associated with a reservoir is no guarantee of producibility (Simm *et al.*, 2014). Therefore further studies including 3D deep seismic are required to better delineate the lenticular structure, together with long-term acoustic monitoring to detect possible gas seeps on the seafloor (particularly in the outer Gulf) and organic geochemical analyses to identify the origin of the gases.

CONCLUSIONS

This paper presents an analysis of multi-channel seismic reflection data to investigate the Miocene – Quaternary stratigraphy of the Gulf of İzmir, western Anatolia. The study provides new insights into the hydrocarbon potential of this area and tentatively identifies a possible hydrocarbon trap within the Plio-Quaternary sedimentary succession. Major conclusions can be summarized as follows:

1. Reflection tomography provides new insights into variations in the two-dimensional P-wave velocity and morphology of sedimentary units down to depths

of 1.75 km in the study area. The model assisted with the stratigraphic interpretation of the area in the depth domain. Two sedimentary units (SSU1 and SSU2) with varying thicknesses overlying the acoustic basement (SSU3) were identified. These units were correlated with Upper Miocene – Pliocene to Recent formations identified at the offshore Foça-1 well.

2. The velocity-depth model and PSDM results demonstrate the existence of a lenticular-shaped low-velocity zone (1.68 km/s) at ~400 m depth with a length of ~500 m and width of ~90 m in the SSU1c sub-unit. AVO analysis, modelling and seismic attributes showed the presence of possible DHIs at the top and base of this structure which are interpreted as bright and flat spots respectively. Based on these observations, a potential reservoir consisting of conglomerates and sandstones is tentatively identified in the Quaternary Bayramiç Formation.

3. The reservoir is sealed by the shales of the Bayramiç Formation above, and is bounded by an unconformity at the base together with strike-slip faults on either side. Therefore the structure may form a structural-stratigraphic trap.

4. The bounding strike-slip faults may allow the migration of hydrocarbons from source rocks at greater depths into the reservoir. The presence of another LVZ above the reservoir along the strike-slip faults may indicate upward leakage towards the seafloor.

ACKNOWLEDGEMENTS

This study is derived from a Ph.D thesis by the first author which is supported by Istanbul Technical University Research Fund (İTÜ-FBE-BAP Project No:39685). The data was collected under the collaboration of ITU-TUBITAK-MTA Research Project No:100Y084. We thank the captain and crew of the MTA Sismik-1 research vessel for their efforts during data acquisition. The study was partly supported by TRILL Fellowship Program of ICTP (visiting scholar during May-August 2016, OGS, Trieste, Italy). We gratefully acknowledge support by the Istituto Nazionale di Oceanografia e di Geofisica Sperimentale (OGS) for allowing us to use the CAT3D software and their laboratories. We thank Bozkurt Çiftçi (*Genel Energy*) whose comments and suggestions during JPG review greatly improved the manuscript. We also thank Nur Schuba for proof reading and for comments on an earlier version of the manuscript, and Stefano Picotti for the comments and suggestions on AVO analysis. We also gratefully acknowledge the Emerson-Paradigm Software Grant for Istanbul Technical University which enabled data processing with their software package Echos™. QGIS software was used by the authors to prepare some of figures.

REFERENCES

AKSOY, N., SERPEN, U. and FILIZ, Ş., 2008. Management of the Balcova–Narlidere geothermal reservoir, Turkey. *Geothermics,* **37**, 444–466.

AKSU, A. E., PIPER, D. J. W. and KONUK, T., 1987. Late Quaternary tectonic and sedimentary history of outer Izmir and Candarli bays, western Turkey. *Marine Geology,* **76**, 89–104.

ALTAN, Z. and OCAKOĞLU, N., 2016. Shallow seismic study of the geothermal areas in the Gülbahçe Bay and Izmir Gulf (Aegean Sea, Western Turkey). *Marine Geophysical Research*, **37**, 297–311.

ATES, A., BILIM, F., BUYUKSARAC, A., AYDEMIR, A., BEKTAS, O. and ASLAN, Y., 2012. Crustal Structure of Turkey from Aeromagnetic, Gravity and Deep Seismic Reflection Data. *Surveys in Geophysics,* **33**, 869–885.

BILIM, F., AKAY, T., AYDEMIR, A. and KOSAROGLU, S., 2016. Curie point depth, heat-flow and radiogenic heat production deduced from the spectral analysis of the aeromagnetic data for geothermal investigation on the Menderes Massif and the Aegean Region, western Turkey. *Geothermics*, **60**, 44–57.

BISHOP, T. N., BUBE, K. P., CUTLER, R. T., LANGAN, R. T., LOVE, P. L., RESNICK, J. R., SHUEY, R. T., SPINDLER, D. A. and WYLD, H. W., 1985. Tomographic determination of velocity and depth in laterally varying media. *Geophysics*, **50**, 903–923.

BÖHM, G., ROSSI, G. and VESNAVER, A., 1999. Minimum time ray tracing for {3D} irregular grids. *J. Seism. Expl.*, **8**, 117–131.

BORDING, R. P., GERSZTENKORN, A., LINES, L. R., SCALES, J. A. and TREITEL, S., 1987. Applications of seismic travel-time tomography. *Geophysical Journal of the Royal Astronomical Society,* **90**, 285–303.

BOURBIÉ, T., COUSSY, O. and ZINSZNER, B., 1987. Acoustics of porous media. Editions Technip., Paris.

CARRION, P., MARCHETTI, A., BOEHM, G., PETTENATI, F. and VESNAVER, A., 1993. Tomographic processing of Antarctica's data. *First Break*, **11**, 295–301.

CARSTENS, H., 2005. Gas found in glacial, shallow sands. *GeoExPro*, **4**, 24–25.

CASTAGNA, J. P., 1993. Offset-Dependent Reflectivity – Theory and Practice of AVO Analysis. In: CASTAGNA, J. P. and BACKUS, M. M. (Eds), Investigations in Geophysics Series, vol. 8. Society of Exploration Geophysicists, Tulsa, OK.

ÇIFTÇI, N. B., TEMEL, R. Ö. and TERZIOĞLU, N., 2004. Neogene stratigraphy and hydrocarbon system of the region surrounding the Gulf of Edremit, NW Anatloia, Turkey. *Turkish Association of Petroleum Geologists Bulletin*, **16**, 81–104.

ÇIFTÇI, N. B., TEMEL, R. Ö. and IZTAN, Y. H., 2010. Hydrocarbon occurrences in the western Anatolian (Aegean) grabens, Turkey: Is there a working petroleum system? *AAPG Bulletin*, **94**, 1827–1857.

CLAERBOUT, J. F., 1985. Imaging the earth's interior. Vol. 1. Blackwell scientific publications, Stanford, California, USA.

COHEN, J. K. and STOCKWELL, J. W., 2003. Seismic Unix Release 37: a free package for seismic research and processing. Center for Wave Phenomena, Colorado School of Mines.

COHEN, J. K. and STOCKWELL, J. W., 2015. Seismic Unix Release 44: a free package for seismic research and processing. Center for Wave Phenomena, Colorado School of Mines.

COSKUN, S., DONDURUR, D., CIFCI, G., AYDEMIR, A. and DRAHOR, M. G., 2016. Natural and anthropogenic submarine morphologies revealed by high resolution acoustic data in the Gulf of Izmir, western Turkey. *Marine and Petroleum Geology,* **71**, 211–224.

DEWEY, J. F. and ŞENGÖR, A. M. C., 1979. Aegean and surrounding regions: Complex multiplate and continuum tectonics in a convergent zone. *Geological Society of America Bulletin,* **90,** 84–92.

DONDURUR, D., ÇIFÇI, G., DRAHOR, M. G. and COŞKUN, S., 2011. Acoustic evidence of shallow gas accumulations and active pockmarks in the Izmir Gulf, Aegean sea. *Marine and Petroleum Geology*, **28**, 1505–1516.

DRAHOR, M. G. and BERGE, M. A., 2006. Geophysical investigations of the Seferihisar geothermal area, Western Anatolia, Turkey. *Geothermics*, **35,** 302–320.

DÜŞÜNÜR-DOĞAN, D. and ÜNER, S., 2019. Numerical simulation of groundwater flow and temperature distribution in Aegean Coast of Turkey. *Journal of Earth System Science*, **128**.

EMRE, Ö., ÖZALP, S., DOĞAN, A., ÖZAKSOY, V., YILDIRIM, C. and GÖKTAŞ, F., 2005. Izmir Yakın Çevresinin Diri Fayları ve Deprem Potansiyelleri (Rapor No: 10754). Ankara: MTA Jeoloji Etütleri Dairesi.

FILIZ, Ş. and TARCAN, G., 1993. Hydrogeology of geothermal area in the south of Seferihisar (Izmir). *TPJD Bült.*, **5**, 97–112.

FORREST, M., RODEN, R. and HOLEYWELL, R., 2010. Risking seismic amplitude anomaly prospects based on database trends. *The Leading Edge*, **29,** 570–574.

GENÇ, C. Ş., ALTUNKAYNAK, Ş., KARACIK, Z., YAZMAN, M. and YILMAZ, Y., 2001. The Çubukludağ graben, south of Izmir: its tectonic significance in the Neogene geological evolution of the western Anatolia. *Geodinamica Acta,* **14,** 45–55.

GÜRGEY, K., SIMONEIT, B. R. T., BATI, Z., KARAMANDERESI, I. H. and VAROL, B., 2007. Origin of petroliferous bitumen from the Büyük Menderes–Gediz geothermal graben system, Denizli – Sarayköy, western Turkey. *Applied Geochemistry*, **22**, 1393–1415.

HAMILTON, E. L., 1978. Sound velocity–density relations in sea-floor sediments and rocks. *The Journal of the Acoustical Society of America*, **63**, 366–377.

HEGGLAND, R., 1998. Gas seepage as an indicator of deeper prospective reservoirs. A study based on exploration 3D seismic data. *Marine and Petroleum Geology*, **15**, 1–9.

HUVAZ, O., SARIKAYA, H. and NOHUT, O. M., 2005. Nature of a regional dogleg pattern in maturity profiles from Thrace basin, northwestern Turkey: A newly discovered unconformity or a thermal anomaly? *AAPG Bulletin*, **89,** 1373–1396.

ILKIŞIK, O. M., 1995. Regional heat flow in western Anatolia using silica temperature estimates from thermal springs. *Tectonophysics*, **244**, 175–184.

IMREN, C., LE PICHON, X., RANGIN, C., DEMIRBAĞ, E., ECEVITOĞLU, B. and GÖRÜR, N., 2001. The North Anatolian Fault within the Sea of Marmara: a new interpretation based on multi-channel seismic and multi-beam bathymetry data. *Earth and Planetary Science Letters,* **186**, 143–158.

KAYSERI-ÖZER, M. S., PEKÇETINÖZ, B. and ÖZEL, E., 2014. Palaeoenvironmental and palynological study of the geothermal area in the Gülbahçe Bay (Aegean Sea, western Turkey). In BABA, A., BUNDSCHUH, J., CHANDRASEKHARAM, D. (Ed.), Geothermal Systems and Energy Resources: Turkey and Greece. CRC Press, EH Leiden, The Netherlands, 305–322 pp.

KJARTANSSON, E., 1979. Modeling and migration by the monochromatic 45-degree equation. Stanford Exploration Project Report No. 15, Stanford University.

McCLUSKY, S., BALASSANIAN, S., BARKA, A., DEMIR, C., ERGINTAV, S., GEORGIEV, I., GURKAN, O., HAMBURGER, M., HURST, K., KAHLE, H., KASTENS, K., KEKELIDZE, G., KING, R., KOTZEV, V., LENK, O., MAHMOUD, S., MISHIN, A., NADARIYA, M., OUZOUNIS, A., PARADISSIS, D., PETER, Y., PRILEPIN, M., REILINGER, R., SANLI, I., SEEGER, H., TEALEB, A., TOKSÖZ, M. N. and VEIS, G., 2000. Global Positioning System constraints on plate kinematics and dynamics in the eastern Mediterranean and Caucasus. *Journal of Geophysical Research: Solid Earth,* **105**, 5695–5719.

McKENZIE, D., 1972. Active Tectonics of the Mediterranean Region. *Geophysical Journal International,* **30,** 109–185.

OCAKOĞLU, N., DEMIRBAĞ, E. and KUŞÇU, I., 2005. Neotectonic structures in Izmir Gulf and surrounding regions (western Turkey): Evidences of strike-slip faulting with compression in the Aegean extensional regime. *Marine Geology*, **219,** 155–171.

OSTRANDER, W. J., 1984. Plane-wave reflection coefficients for gas sands at nonnormal angles of incidence. *Geophysics,* **49**, 1637–1648.

PAMUKÇU, O., GÖNENÇ, T., SINDIRGI, P. and BABA, A., 2014. Application of geophysical methods in Gulbahce geothermal site, Urla-Izmir, western Anatolia. Geothermal Systems and Energy Resources: Turkey and Greece, 251.

PEKÇETINÖZ, B., 2010. Izmir ve civar körfezlerdeki jeotermal alanların araştırılması (Gülbahçe körfezi örneginde). DEÜ Fen Bilimleri Enstitüsü, 191pp.

PERINCEK, D., 1991. Possible Strand of the North Anatolian Fault in the Thrace Basin, Turkey - An Interpretation (1). *AAPG bulletin,* **75**, 241–257.

LE PICHON, X., ANGELIER, J., OSMASTON, M. F. and STEGENA, L., 1981. The Aegean Sea [and Discussion]. *Philosophical Transactions of the Royal Society of London. Series A, Mathematical and Physical Sciences,* **300**, 357–372.

LE PICHON, X., CHAMOT-ROOKE, N., LALLEMANT, S., NOOMEN, R. and VEIS, G., 1995. Geodetic determination of the kinematics of central Greece with respect to Europe: Implications for eastern Mediterranean tectonics. *Journal of Geophysical Research: Solid Earth*, **100,** 12675–12690.

PROEDROU, P. and SIDIROPOULOS, T., 1992. Prinos Field–Greece. Aegean basin. In: Structural Traps. *AAPG Treatise of Petroleum Geology, Atlas of oil and gas fields,* **6,** 275–291. AAPG, Tulsa.

QGIS DEVELOPMENT TEAM, 2012. QGIS Geographic Information System. Open Source Geospatial Foundation Project http://qgisosgeoorg.

REILINGER, R. E., McCLUSKY, S. C., ORAL, M. B., KING, R. W., TOKSOZ, M. N., BARKA, A. A., KINIK, I., LENK, O. and SANLI, I., 1997. Global Positioning System measurements of present-day crustal movements in the Arabia-Africa-Eurasia plate collision zone. *Journal of Geophysical Research: Solid Earth,* **102**, 9983–9999.

RUTHERFORD, S. R. and WILLIAMS, R. H., 1989. Amplitude-versus-offset variations in gas sands. *Geophysics,* **54**, 680–688.

ŞAROĞLU, F., EMRE, Ö. and KUŞÇU, I., 1992. Active fault map of Turkey. General Directorate of Mineral Research and Exploration, Ankara.

ŞENGÖR, A. M. C., GÖRÜR, N. and ŞAROĞLU, F., 1985. Strike-Slip Faulting and Related Basin Formation in Zones of Tectonic Escape: Turkey as a Case Study. In: BIDDLE, K. and CHRISTIE-BLICK, N. (Eds), Strike-Slip Deformation, Basin Formation, and Sedimentation. Society of Economic Paleontologists and Mineralogists, 227–264 pp.

SIMM, R., BACON, M. and BACON, M., 2014. Seismic Amplitude: An interpreter's handbook. Cambridge University Press.

SIYAKO, M. and HUVAZ, O., 2007. Eocene stratigraphic evolution of the Thrace Basin, Turkey. *Sedimentary Geology,* **198**, 75–91.

STEWART, R. R., 1991. Exploration Seismic Tomography: Fundamentals. Society of Exploration Geophysicists, Tulsa, USA.

STORK, C., 1992. Reflection tomography in the postmigrated domain. *Geophysics,* **57**, 680–692.

TANER, M. T. and SHERIFF, R. E., 1977. Application of amplitude, frequency and other attributes to stratigraphic and hydrocarbon determination. In: Peyton, C.E. (Ed.), Seismic Stratigraphy – applications to hydrocarbon exploration. *AAPG Memoir* **26**, 301-327. AAPG, Tulsa, OK.

TANER, M. T. and BAYSAL, E., 1993. Velocity Analysis and Depth Migration of Complex Structures. In: Ozan Sungurlu

Symposium Proceedings, Tectonics and Hydrocarbon Potential of Anatolia and Surrounding Regions, November 1991, Anakara, Türkiye. pp 138–155.

TARCAN, G., GEMICI, Ü. and AKSOY, N., 2005. Hydrogeological and geochemical assessments of the Gediz Graben geothermal areas, western Anatolia, Turkey. *Environmental Geology*, **47**, 523–534.

TAYMAZ, T., JACKSON, J. and McKENZIE, D., 1991. Active tectonics of the north and central Aegean Sea. *Geophysical Journal International*, **106**, 433–490.

TOKÇAER, M., AGOSTINI, S. and SAVAŞÇIN, M. Y., 2005. Geotectonic setting and origin of the youngest Kula volcanics (western Anatolia), with a new emplacement model. *Turkish Journal of Earth Sciences*, **14**, 143–166.

ÜNER, S., AĞAÇGÖZGÜ, G. Ö. and DOĞAN, D. D., 2019. Hydrogeophysical modelling of Hisarcik (Kütahya) geothermal field, western Turkey. *Geophysical Prospecting*, **67,** 2176–2195.

USTAÖMER, T., GÖKAŞAN, E., TUR, H., GÖRÜM, T., BATUK, F. G., KALAFAT, D., ALP, H., ECEVITOĞLU, B. and BIRKAN, H., 2008. Faulting, mass-wasting and deposition in an active dextral shear zone, the Gulf of Saros and the NE Aegean Sea, NW Turkey. *Geo-Marine Letters*, **28**, 171–193.

YILMAZ, Y., GENÇ, Ş. C., KARACIK, Z. and ALTUNKAYNAK, Ş., 2001. Two contrasting magmatic associations of NW Anatolia and their tectonic significance. *Journal of Geodynamics*, **31**, 243–271.

YILMAZ, Y., GENC, S. C., GURER, F., BOZCU, M., YILMAZ, K., KARACIK, Z., ALTUNKAYNAK, S. and ELMAS, A., 2000. When did the Western Anatolian grabens begin to develop? In: BOZKURT, E., WINCHESTER, J. A. and PIPER, J.D.A. (Eds), Tectonics and Magmatism in Turkey and the Surrounding Area. *Geol. Soc. Lond., Spec. Publ.* **173**, 353-384.

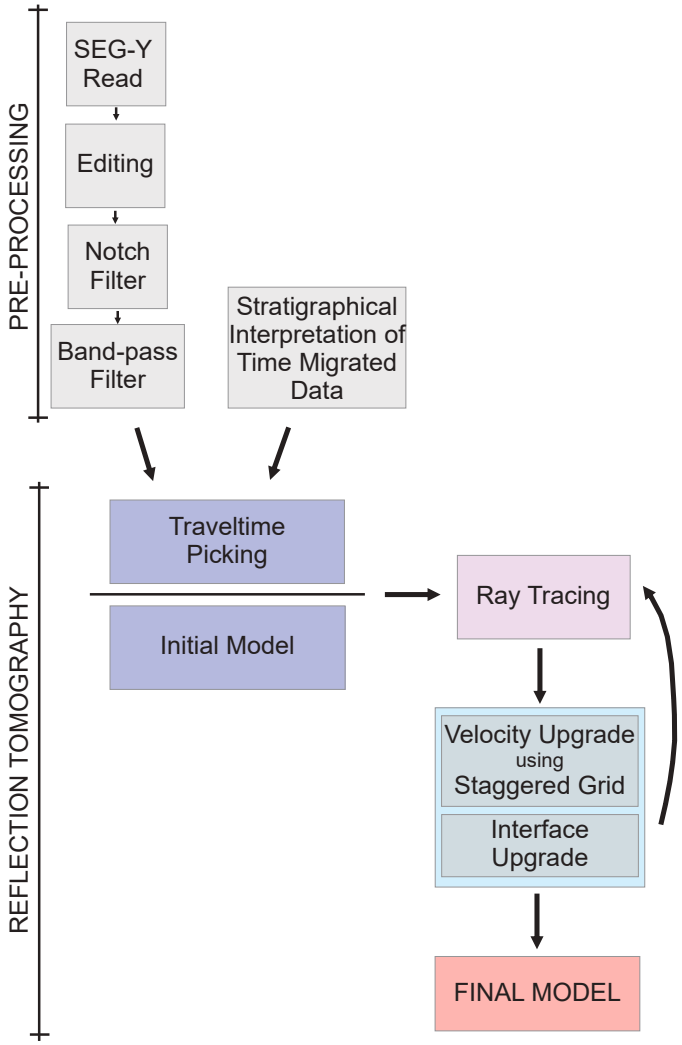

Appendix Fig. 1. Workflow used in this study for the tomographic inversion procedure for the reflected arrivals. Due to the excessive background noise on the pre-stack data, various pre-processing steps were required to assist with accurate picking. Pre-processing steps are also pesented in the flow chart.